Self-Assembly of Diblock Copolymer Mixtures in Confined States: A Monte Carlo Study

2 AUTHORS, INCLUDING:

Yutian Zhu

Chinese Academy of Sciences

43 PUBLICATIONS **356** CITATIONS

Self-Assembly of Diblock Copolymer Mixtures in Confined States: A Monte Carlo Study

Yutian Zhu[†,‡] and Wei Jiang*,[†]

State Key Laboratory of Polymer Physics and Chemistry, Changchun Institute of Applied Chemistry, Chinese Academy of Sciences, Changchun 130022, P. R. China, and Graduate School of the Chinese Academy of Sciences

ABSTRACT: The self-assembly of diblock copolymer mixtures (A-*b*-B/A-*b*-C or A-*b*-B/B-*b*-C mixtures) subjected to cylindrical confinement (two-dimensional confinement) was investigated using a Monte Carlo method. In this study, the boundary surfaces were configured to attract blocks A but repel blocks B and C. Relative to the structures of the individual components, the self-assembled structures of mixtures of the diblock copolymers were more complex and interesting. Under cylindrical confinement, with varying cylinder diameters and interaction energies between the boundary surfaces and the blocks, we observed a variety of interesting morphologies. Upon decreasing the cylinder's diameter, the self-assembled structures of the $A_{15}B_{15}/A_{15}C_{15}$ mixtures changed from double-helix/cylinder structures (blocks B and C formed double helices, whereas blocks A formed the outer barrel and inner core) to stacked disk/cylinder structures (blocks B and C formed the stacked disk core, blocks A formed the outer cylindrical barrel), whereas the self-assembled structures of the $A_{15}B_7/B_7C_{15}$ mixtures changed from concentric cylindrical barrel structures to screw/cylinder structures (blocks C formed an inside core winding with helical stripes, whereas blocks A and B formed the outer cylindrical barrels) and then finally to the stacked disk/cylinder structures. In contrast, increasing the interaction energy between the boundary surfaces and the blocks, the self-assembled structures of the $A_{15}B_{15}/A_{15}C_{15}$ mixtures changed from stacked disk structures (sequence of alternating A and BC disks) to BC stacked sphere/cylinder structures (the core was connected by B and C spheres in an alternating sequence) and then to the stacked disk/cylinder structures, whereas the self-assembled structures of the $A_{15}B_7/B_7C_{15}$ mixtures changed from stacked disk structures (sequence of alternating of A, B, and C disks) to catenoid/cylinder structures (B blocks formed a bottleneck structure connecting the separate cylindrical BC domains) and then to the stacked disk/cylinder structures. Moreover, we have analyzed the self-assembled structures in terms of chain conformation and given the chain packing models for various self-assembled structures.

1. Introduction

Self-assembly in macromolecular systems is a powerful method for creating novel phase structures on the nanoscale. Polymeric materials possessing novel structures should exhibit novel physical properties and have a variety of potential applications.[1] Confinement effects, imposed by boundary surfaces, can lead to some unique phase structures that are quite different from those obtained under classical equilibrium behavior. Therefore, the phase behavior of block copolymers in confined systems has received a great deal of attention. For instance, the microphase separation of block copolymers confined between two parallel walls has been studied extensively.[2−8] Recently, Russell and co-workers investigated the self-assembly of polystyrene-*block*-polybutadiene (PS-*b*-PBD) copolymers confined within cylindrical nanopores in alumina membranes; they observed multiple concentric cylindrical barrel structures,[9,10] stacked torus-type structures,[11] helical strings of spherical structures,[11] as well as stacked disk[9] and helical[12] morphologies in the pores. Similarly, Sun et al.[13] examined the phase behavior of polystyrene-*block*-poly(methyl methacrylate) (PS-*b*-PMMA) confined within alumina nanopores; they also observed concentric cylindrical barrel structures. In a theoretical study, Liang et al.[14] performed Monte Carlo simulations to investigate symmetric block copolymers in spherical and cylindrical confinements. Sevink et al.[15] applied dynamic density functional theory to investigate the effect of cylindrical confinements on the morphology of a symmetric diblock copolymer system. Li et al.[16] used real-space self-consistent mean-field theory to explore the phase diagram of a diblock copolymer melt confined within cylindrical nanopores. Yu et al.[17] studied the self-assembly of block copolymers in cylindrical nanopores by using Monte Carlo simulation. They pointed out that the formations of the self-assembled structure depended on the pore diameter and the surface−polymer interactions. More recently, Feng et al.[18] employed Monte Carlo simulations to investigate the morphologies of symmetrical AB diblock copolymer melts under the confinement of nanocylindrical tubes.

Although most studies in this field to date have focused on the self-assembly of individual block copolymers in the bulk and confinement, the self-assembly of mixtures of two or more block copolymers in solution has also been studied. To the best of our knowledge, however, the self-assembly of block copolymer mixtures under cylindrical or spherical confinement has not yet been reported. In this study, we used the Monte Carlo method to systematically investigate the self-assembly of mixtures of diblock copolymers under cylindrical confinement; we found a rich range of novel self-assembled structures that may aid in the design of novel polymeric nanomaterials under confinement.

2. Model and Simulation

Monte Carlo simulation was performed in a three-dimensional lattice having a cylindrical boundary in which various interac-
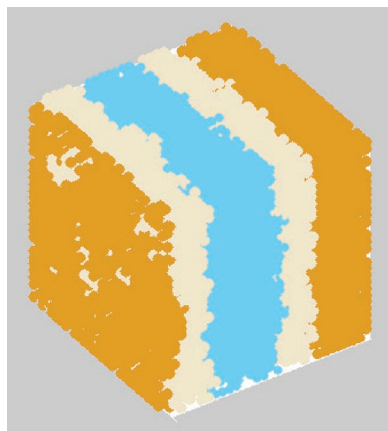
* Corresponding author. E-mail: wjiang@ciac.jl.cn. Telephone: +86-431-85262151. Fax: +86-431-85262126.
† State Key Laboratory of Polymer Physics and Chemistry, Changchun Institute of Applied Chemistry.
‡ Graduate School of the Chinese Academy of Sciences.
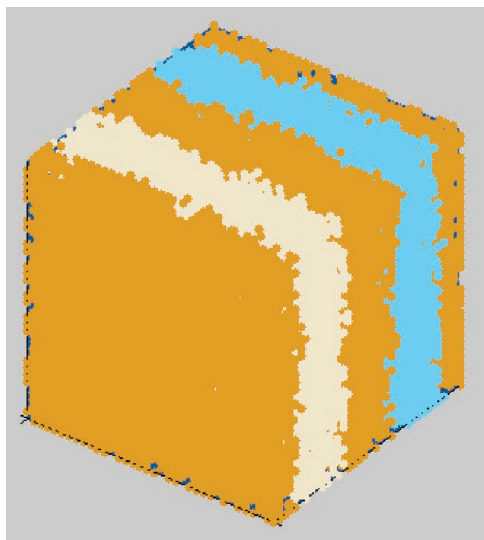
Figure 1. Morphological pattern formed from $A_{15}B_{15}/A_{15}C_{15}$ mixtures in a $36 \times 36 \times 36$ lattice.


Figure 2. Morphological pattern formed from $A_{15}B_7/B_7C_{15}$ mixtures in a $30 \times 30 \times 30$ lattice.

tions existed between the boundary and the diblock copolymers. The self-assembly of both $A_{15}\text{-}b\text{-}B_{15}/A_{15}\text{-}b\text{-}C_{15}$ and $A_{15}\text{-}b\text{-}B_7/B_7\text{-}b\text{-}C_{15}$ mixtures was considered. The component ratios for the two mixtures were fixed at 50/50, respectively. The volume fraction of the mixtures of diblock copolymers was fixed at 0.7. In all cases, the chain number of $A_{15}\text{-}b\text{-}B_{15}$ copolymers was always equal to that of $A_{15}\text{-}b\text{-}C_{15}$ copolymers in the $A_{15}\text{-}b\text{-}B_{15}/A_{15}\text{-}b\text{-}C_{15}$ mixtures, and the chain number of $A_{15}\text{-}b\text{-}B_7$ copolymers was always equal to that of $B_7\text{-}b\text{-}C_{15}$ in the $A_{15}\text{-}b\text{-}B_7/B_7\text{-}b\text{-}C_{15}$ mixtures. In present study, the main purpose is to study the effects of pore diameter and the interactions between the boundary surface and the blocks. Therefore, the cylinder length was chosen to be 180 in most cases. However, we had to choose the cylinder length to be 60 when the cylinder diameter was 60 because the simulation time was too long to be tolerated if we also chose the cylinder length to be 180 in this case. In addition, the period boundary condition[19] was imposed in the cylinder axis direction to mimic long cylinder. Attractive interactions existed between the boundary and block A; repulsive interactions existed between the boundary and both blocks B and C. Because of the high concentration of polymer segments, the "single-site bond fluctuation model", proposed by Larson et al.[20,21] and Carmesin et al.,[22] was employed in these simulations. The chain configuration was evolved during the course of the Monte Carlo simulations by attempting random displacements of a single vacancy site to the 18 nearest-neighbor site beads in the lattice.
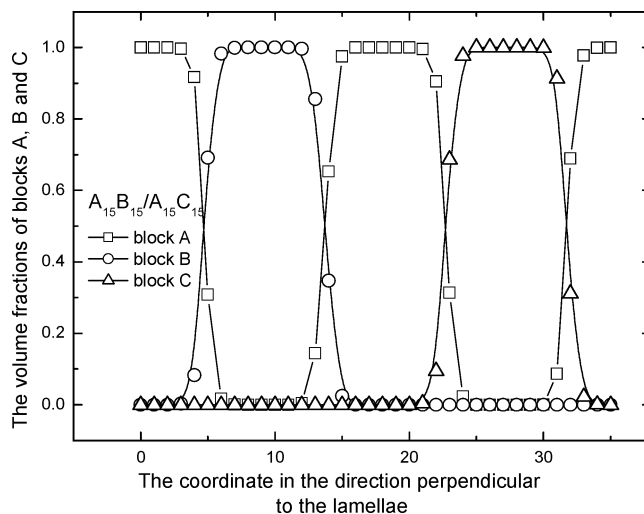
Figure 3. Variations of the volume fractions of blocks A, B, and C along the direction perpendicular to the lamellae.
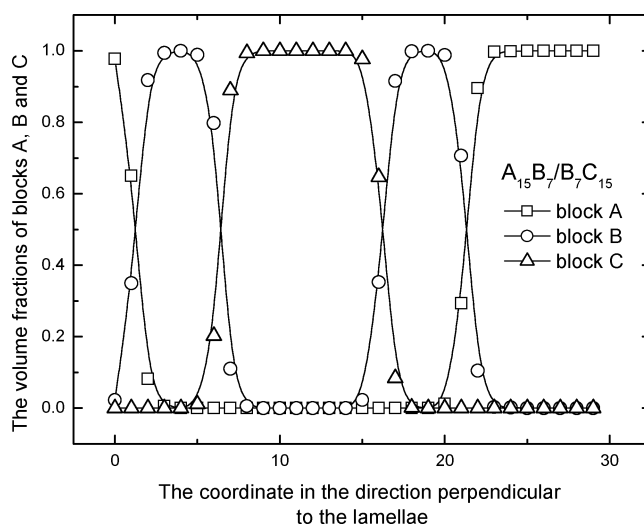

Figure 4. Variations of the volume fractions of blocks A, B, and C along the direction perpendicular to the lamellae.
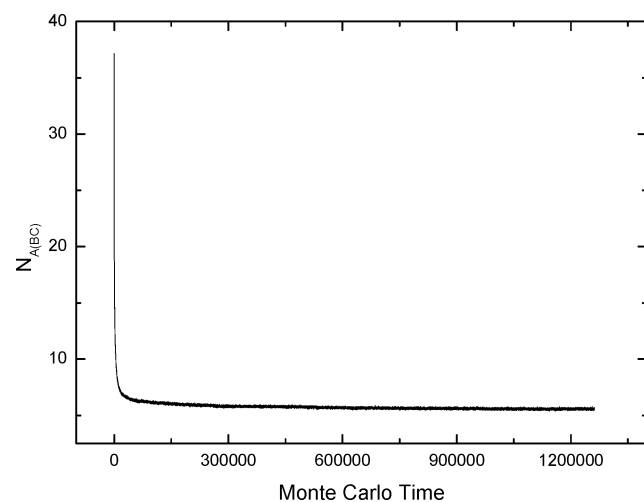
Figure 5. Variations of contact numbers of A−BC pairs of segments with Monte Carlo time for the $A_{15}B_{15}/A_{15}C_{15}$ mixtures.

These attempted moves changed the lengths of the bonds within the chain; the chain connectivity was maintained by restricting the bond lengths to values of 1 and $\sqrt{2}$. Excluded volume interactions were enforced to assume that no more than one bead existed per lattice site. No bond crossing was allowed. If
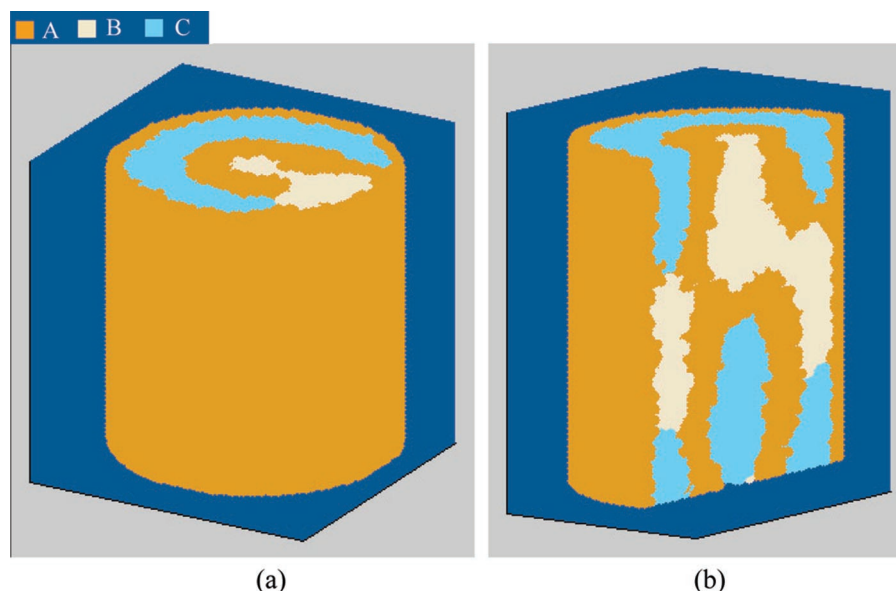
Figure 6. Morphological patterns formed from $A_{15}B_{15}/A_{15}C_{15}$ mixtures within a cylindrical boundary. (a) Three-dimensional structure; (b) section structure. Both the height and diameter of the cylinder were 60. The blue area is the background.
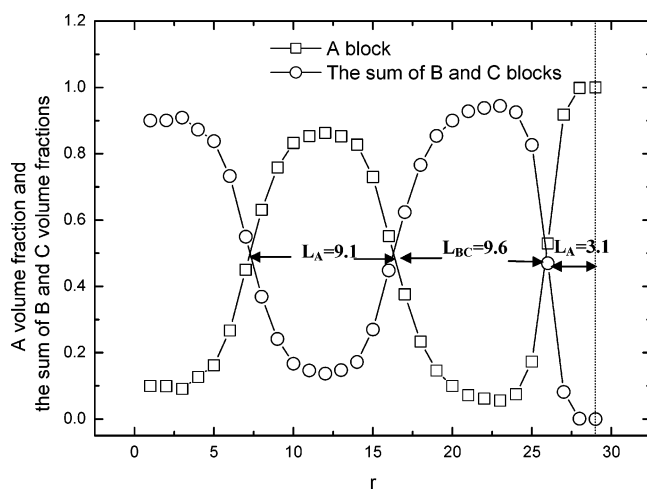
Figure 7. Variations of the A volume fraction and the sum of the B and C volume fractions along the cylinder radius (r).

the attempted move violated the excluded volume condition, or the no bond-crossing, or bond length restrictions, then it was rejected. Attempted moves that satisfied both the excluded volume condition and the bond length restrictions were accepted or rejected according to Metropolis rules,[23] i.e., an attempted move was accepted if the energy change ΔE was negative, or accepted with probability $p = \exp(-\Delta E/(kT))$, if ΔE was positive, where $\Delta E = (\Delta N_{AA}\epsilon_{AA} + \Delta N_{BB}\epsilon_{BB} + \Delta N_{CC}\epsilon_{CC} + \Delta N_{AB}\epsilon_{AB} + \Delta N_{AC}\epsilon_{AC} + \Delta N_{BC}\epsilon_{BC} + \Delta N_{AD}\epsilon_{AD} + \Delta N_{BD}\epsilon_{BD} + \Delta N_{CD}\epsilon_{CD})$ is the change in energy that accompanied the attempted move, ΔN is the difference between the number of nearest-neighboring pairs of the sites occupied by monomers or by boundaries before and after movement, ϵ is the interaction energy that was won if two neighboring lattice sites are taken by monomers or boundaries, and the subscripts A−D denote monomers A, B, and C and the boundary units, respectively.

In the simulation, $\bar{\epsilon}$ ($\bar{\epsilon} = \epsilon/(kT)$) is the reduced interaction energy. First, the system was annealed in an athermal state for a sufficiently long time to reach an equilibrium disorder state. Next, we set the following values, $\overline{\epsilon_{AA}} = \overline{\epsilon_{BB}} = \overline{\epsilon_{CC}} = 0$, $\overline{\epsilon_{AB}} = \overline{\epsilon_{AC}} = \overline{\epsilon_{BC}} = 0.5$, $\overline{\epsilon_{AD}} = -\epsilon_1$, $\overline{\epsilon_{BD}} = \overline{\epsilon_{CD}} = \epsilon_1$ ($\epsilon_1 \geq 0$), to ensure that blocks A, B, and C would be immiscible with each

other and that the boundary would attract block A but repulse both blocks B and C. In this study, ϵ_1 was fixed at a value of 1, except in one investigation into its effect on self-assembled morphologies.

3. Results and Discussion

In order to probe the lamellae period (L_0) of $A_{15}B_{15}/A_{15}C_{15}$ and $A_{15}B_7/B_7C_{15}$ mixtures in bulk states, we first obtained the morphological patterns of $A_{15}B_{15}/A_{15}C_{15}$ mixtures in a $36 \times 36 \times 36$ lattice and $A_{15}B_7/B_7C_{15}$ mixtures in a $30 \times 30 \times 30$ lattice, as shown in Figures 1 and 2. The period boundary condition was imposed in X, Y, and Z directions to mimic a bulk system. We set $\overline{\epsilon_{AA}} = \overline{\epsilon_{BB}} = \overline{\epsilon_{CC}} = 0$ and $\overline{\epsilon_{AB}} = \overline{\epsilon_{AC}} = \overline{\epsilon_{BC}} = 0.5$. It can be seen that the $A_{15}B_{15}/A_{15}C_{15}$ mixtures formed lamellae with a sequence of A-B-A-C (Figure 1), whereas the $A_{15}B_7/B_7C_{15}$ mixtures formed lamellae with a sequence of A-B-C-B (Figure 2). To study the lamellar thicknesses quantitatively, we obtained (Figures 3 and 4) the variations of the volume fractions of blocks A, B, and C along the direction perpendicular to the lamellae. For the $A_{15}B_{15}/A_{15}C_{15}$ mixtures, we found that the thicknesses of the lamellae formed by blocks A, B, and C were ca. 9.0, as shown in Figure 3. However, for the $A_{15}B_7/B_7C_{15}$ mixtures, they formed one thick A and C lamellae (The thickness is ca. 9.0.) and two thin B lamellae (The thickness is ca. 5.0.), as shown in Figure 4. Moreover, it can be found that the bulk period of $A_{15}B_7/B_7C_{15}$ mixture is different from that of $A_{15}B_{15}/A_{15}C_{15}$ mixture. However, the lamellar thicknesses of blocks A and C remains unchanged for the two mixtures. For the purpose of comparability, we chose the thickness ($L_0 = 9.0$) of one layer of block A (or C) to be compared with the cylinder diameter D.

To probe the systems at the equilibrium state, the contact number ($N_{A(BC)}$) was introduced into this work. The definition of $N_{A(BC)}$ is the average number of A and BC pairs of segments within the distance of $\sqrt{2}$ per chain. Similar definitions have been employed by Sariban and Binder in the study of polymer/polymer/solvent mixtures.[24] It is considered that the value of the contact number indicates the miscibility of two polymers; the lower the value of the contact number, the poorer the miscibility of the two polymers is. Because blocks A, B, and C were immiscible with each other, they tended to phase separate into distinct domains, leading to the decrease of $N_{A(BC)}$. Figure
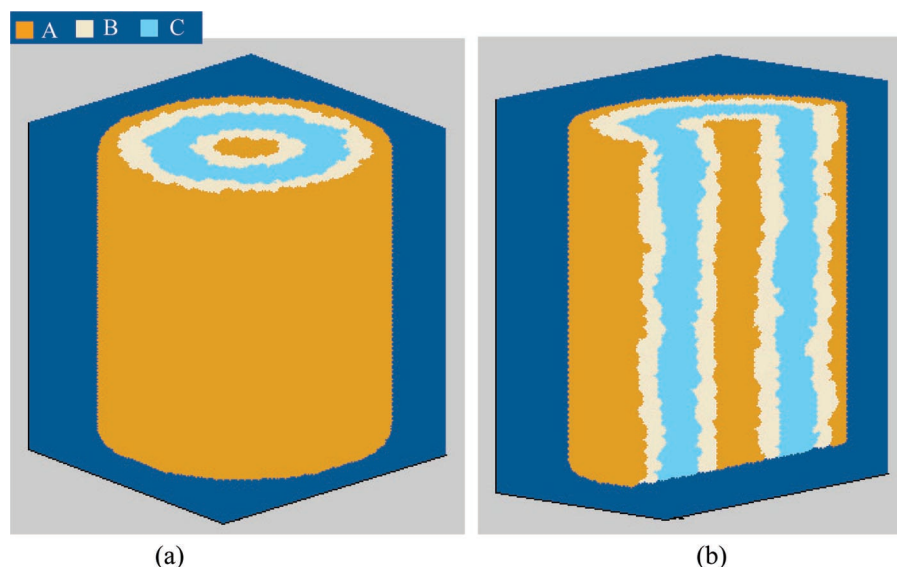
Figure 8. Morphological patterns formed from $A_{15}B_7/B_7C_{15}$ mixtures within a cylindrical boundary. (a) Three-dimensional structure; (b) section structure. Both the height and diameter of the cylinder were 60. The blue area is the background.
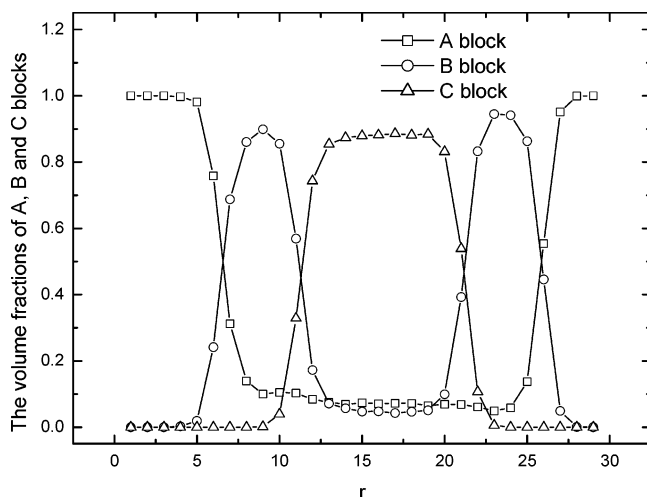
Figure 9. Variations of the volume fractions of blocks A, B, and C along the cylinder radius (r).

5 shows the variation of $N_{A(BC)}$ with Monte Carlo time for the $A_{15}B_{15}/A_{15}C_{15}$ mixtures confined within the cylinder with a diameter of 60. It is seen that $N_{A(BC)}$ decreases considerably with increasing Monte Carlo time up to about 5×10^4, thereafter it almost remains unchanged with further increasing Monte Carlo time. To ensure the structures at equilibrium states, all results presented in this paper were over 8×10^5 Monte Carlo time.

Figure 6 displays the results of simulation of the self-assembled structures of the $A_{15}B_{15}/A_{15}C_{15}$ mixtures in a cylindrically confined state. We observe that the $A_{15}B_{15}/A_{15}C_{15}$ mixtures formed a multiple concentric cylindrical barrel structure that is different to the classical multiple concentric cylindrical barrel structures reported previously.[9,10,12,13] Here, the arrangement sequence of blocks A, B, and C in the self-assembled structure was A-BC-A-BC-A-BC-A. In addition, the BC cylindrical barrels were co-formed by B and C domains with an alternating arrangement sequence. To the best of our knowledge, this structure had previously not been observed either theoretically or experimentally. Because the A blocks were attracted by the cylinder wall, they tended to be close to the cylinder wall and form the outermost cylindrical A barrel. However, the B and C blocks tended to co-form a BC cylindrical barrel due to the chemical bonds of A-B and A-C. As a result, the $A_{15}B_{15}/$

$A_{15}C_{15}$ mixtures formed the multiple concentric cylindrical barrel structure. To study the cylindrical barrel sizes quantitatively, we obtained (Figure 7) the variations of the volume fractions of block A and the sum of blocks B and C along the cylinder radius (r). We found that the thickness of the outermost cylindrical barrel formed by block A was ca. 3.1, whereas the thickness of inside cylindrical barrels was ca. 9.0.

For the sake of comparison, we studied the $A_{15}B_7/B_7C_{15}$ mixtures under the same conditions; Figure 8 presents their morphologies. From the section structure pattern in Figure 8b, we observe that the diblock copolymer mixtures can form a multiple concentric cylindrical barrel structure with an arrangement sequence of A-B-C-B-A-B-C-B-A. Because of the attractive interaction existed between the cylinder boundary and block A, the A blocks of AB diblock copolymers formed the outer A barrel, whereas the B blocks of AB and BC diblock copolymers formed the inner B barrel; the C blocks of BC copolymers formed the third C barrel, and the B blocks of AB and BC copolymers formed the fourth core, and the A blocks of AB copolymers formed the inside core. Similarly, Figure 9 displays the variation of the volume fractions of blocks A, B, and C along the cylinder radius (r). We can see that the thickness of the B barrel is ca. 4.7

The confined size is a key parameter that generally determines the structures of confined polymers. When the cylinder diameter is comparable to the length of the equilibrium period, Russell and co-workers[9,11] proposed that diblock copolymer melts would form unique structures such as the stacked disks and helices. In this study, we also investigated the structures of diblock copolymer mixtures within cylinders of small diameters and discovered some novel structures. Figure 10 displays the structures of $A_{15}B_{15}/A_{15}C_{15}$ mixtures within cylinders of various diameters. When the diameter was 32 ($D/L_0 = 3.6$), the diblock copolymers formed a two-layer concentric cylindrical barrel structure with a sequence of A-BC-A-BC-A, as shown in Figure 10a. In addition, we found that blocks B and C formed some stripes winding around the A core such as the double-helix structure presented in Figure 10a-3 and Figure 10a-4. Elbs et al.[25,26] observed a similar helical structure in thin films of ABC triblock copolymers in which cylindrical A cores were surrounded by helices of B microdomains embedded in a C matrix. In our study, the A core was surrounded by double helices of
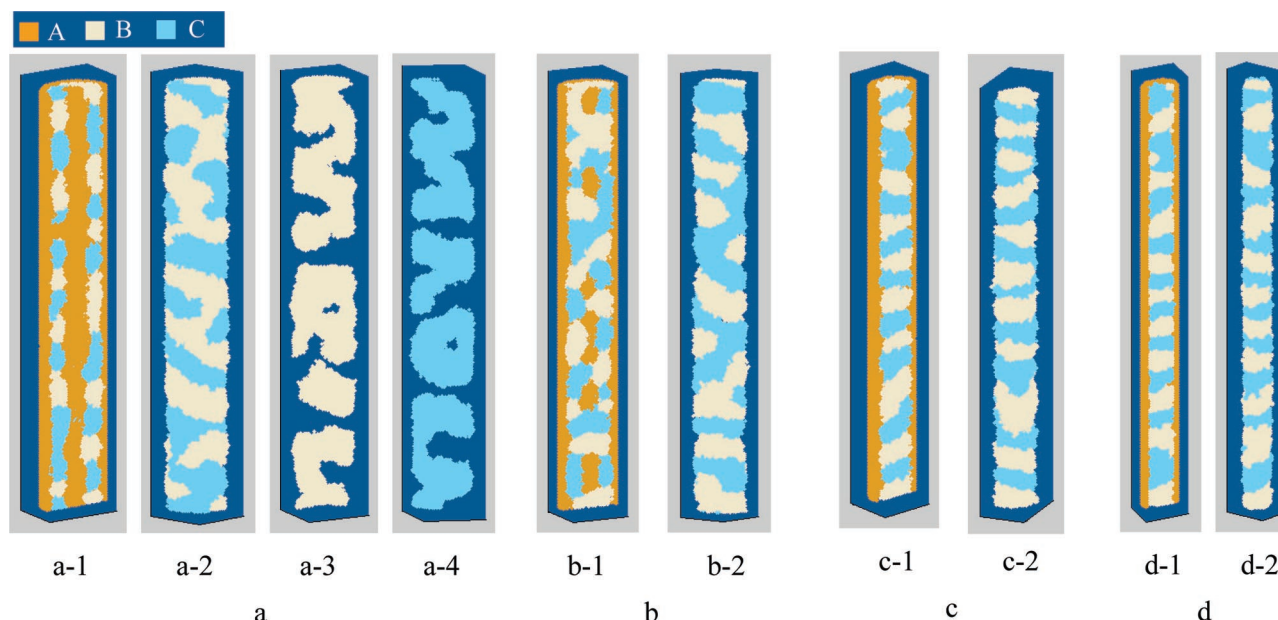
Figure 10. Morphological patterns formed from $A_{15}B_{15}/A_{15}C_{15}$ mixtures constrained within cylinders of various diameters: (a) $D = 32$, (a-1) the section structure, (a-2) only blocks B and C, (a-3) only block B, (a-4) only block C; (b) $D = 28$, (b-1) the section structure, (b-2) only blocks B and C; (c) $D = 24$, (c-1) the section structure, (c-2) only blocks B and C; (d) $D = 16$, (d-1) the section structure, (d-2) only blocks B and C. The cylinder height was 180. The blue area is the background.
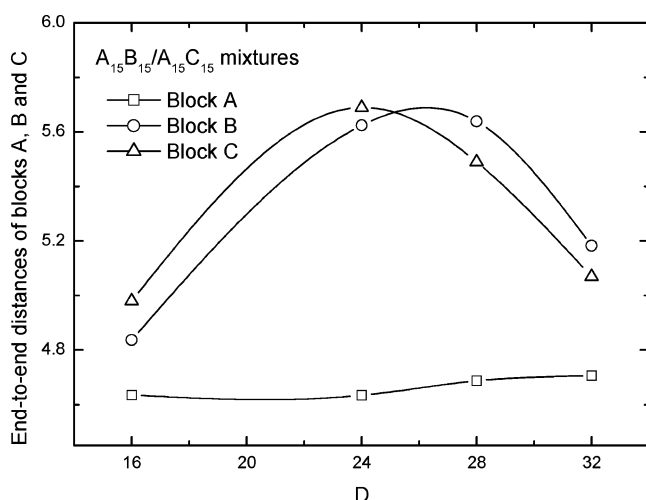

Figure 11. Variations of the end-to-end distances of blocks A, B, and C for the $A_{15}B_{15}/A_{15}C_{15}$ mixtures with the cylinder diameter.
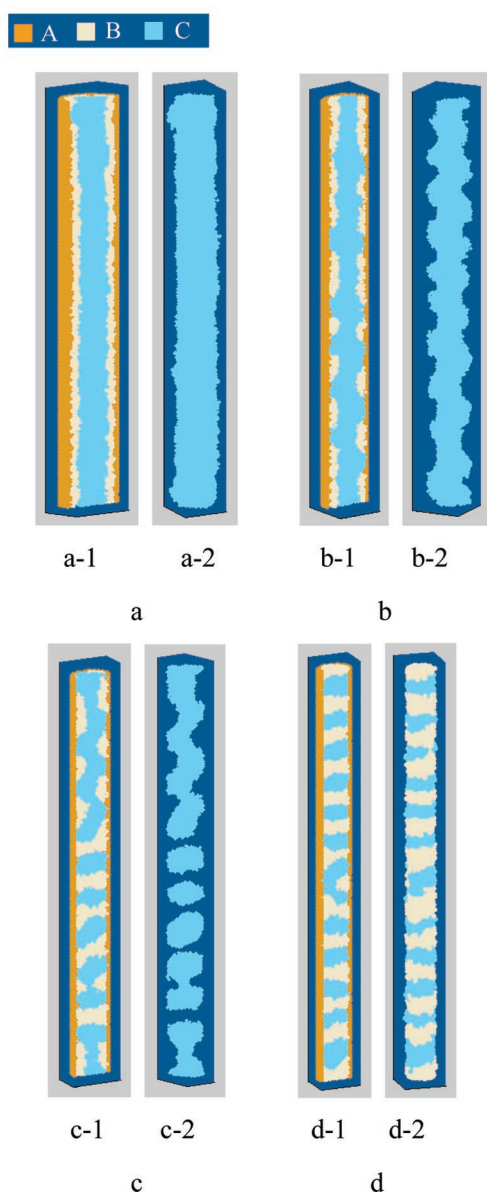
B and C microdomains. This morphology was first observed in the bulk. When the cylinder diameter was less than or equal to 24 ($D/L_0 = <2.7$), however, blocks B and C formed a stacked disk core in the center of the cylinder, whereas blocks A would form an outer cylindrical layer, as indicated in Figure 10c and d. Moreover, these B and C disks were aligned perpendicular to the cylinder axis. We calculated the average thicknesses of B and C disks and found they were ca. 9.0. Russell and co-workers[9] reported a different stacked disk structure that was formed from the melts of polystyrene-*b*-polybutadiene diblock copolymers in a cylindrical pore. In that study, the polybutadiene units assembled into stacked lamellar structures that were aligned perpendicular to the rod axis, whereas the polystyrene units formed a central spine and an outer cylinder. When the diameter was 28 ($D/L_0 = 3.1$), the structure formed from the mixtures of copolymers was a transition structure between the double-helix and stacked disk/cylinder structures (Figure 10b). In the area with high contents of blocks B and C, the B and C blocks formed the stacked disk core in the center of the cylinder; However, in the area with a high content of block A, the A

blocks formed the cylindrical core, and the B and C blocks formed the cylindrical barrel with double-helix structure. In addition, it is necessary to note that block B and C could only separate at a microscopic scale although the B and C components are not grafted on the same chains. This is because the initial state of the system is at equilibrium disorder state, which means that the B and C blocks randomly distributed in the pore. When we add the predetermined energies to the system, block B tends to aggregate to form a small block B domain. Accordingly, a small block C domain can form nearby the small block B domain because B and C blocks are randomly distributed in the pore initially. However, both the block B domain and block C domain cannot increase ceaselessly along the pore axis direction because of the strong confinement and the attraction between block A and the pore boundary. As a result, they can only separate at a microscopic scale although the B and C components are not grafted on the same chains.

It is clear that the phase domain layer sequence along the diameter was A-BC-A-BC-A in the case of $D = 32$ (Figure 10a). The calculated thicknesses for the outermost A, BC, and center A layers were 2.4, 7.0, and 9.2, respectively. In the case of $D = 24$ (Figure 10c), the phase domain layer sequence along the diameter became A-BC-A. The calculated thicknesses for the outermost A and inner BC layers became 2.5 and 15.0, respectively. In the case of $D = 16$ (Figure 10d), the phase domain layer sequence along diameter was still A-BC-A. However, the calculated thicknesses for the outermost A and inner BC layers were 1.5 and 9.0 in this case. This result reveals that the thickness of the outermost A layer is always very thin for various cylinder diameters. On the other hand, the thickness of BC layer increased with decreasing the cylinder diameter from 32 to 24 and then decreased with further decreasing of the cylinder diameter. This result indicates that the conformation of blocks B and C is variable with cylinder diameter. Figure 11 shows the variations of the end-to-end distances of blocks A, B, and C with the cylinder diameter. Clearly, the end-to-end distances of blocks B and C increase with decreasing cylinder diameter at first, and then they decrease with further decreasing cylinder diameter. On the other hand, the end-to-
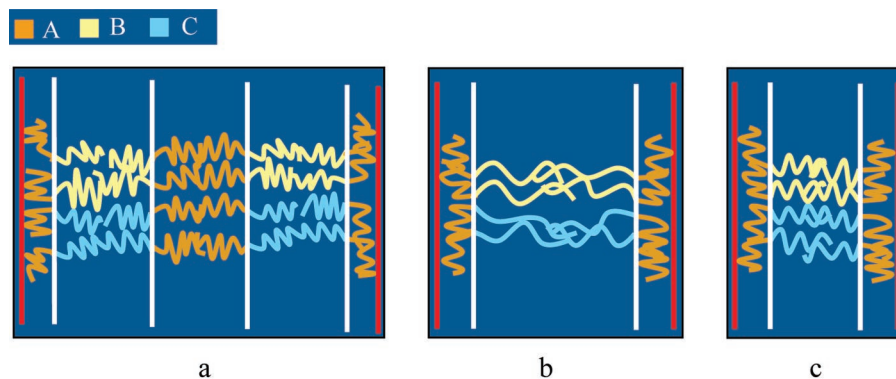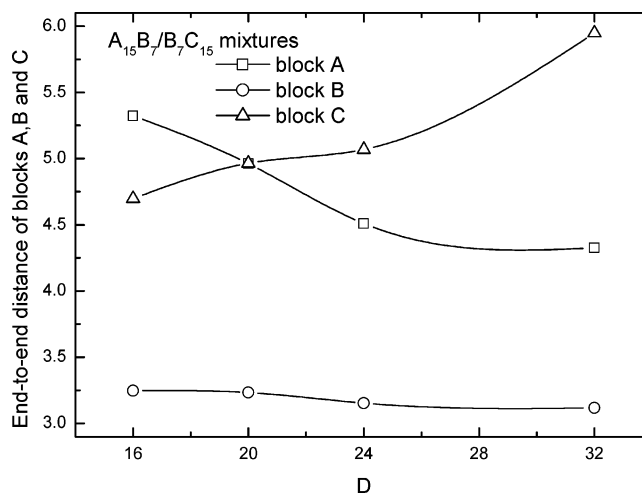
Figure 12. Schematic diagrams of the microstructures of $A_{15}B_{15}/A_{15}C_{15}$ copolymers in the cylinder with various diameters. The red and white lines refer to the cylinder wall and phase interface. (a) $D = 32$; (b) $D = 24$; (c) $D = 16$.

Figure 14. Variations of the end-to-end distances of blocks A, B, and C for the $A_{15}B_7/B_7C_{15}$ mixtures with the cylinder diameter.

Figure 13. Morphological patterns formed from $A_{15}B_7/B_7C_{15}$ mixtures constrained within cylinders of various diameters: (a) $D = 32$, (a-1) the section structure, (a-2) only block C; (b) $D = 24$, (b-1) the section structure, (b-2) only block C; (c) $D = 20$, (c-1) the section structure, (c-2) only block C; (d) $D = 16$, (d-1) the section structure, (d-2) only blocks B and C. The cylinder height was 180. The blue area is the background.

end distance of block A was less than those of blocks B and C. These results suggested that the larger the phase domain, the

higher degree of stretching of the block chain inside was. Based on the above results and discussion, we present a series of schematic illustrations of the microstructures for the $A_{15}B_{15}/A_{15}C_{15}$ mixtures within various cylinders, as shown in Figure 12a−c.

Figure 13 displays another type of morphological transition occurred for the $A_{15}B_7/B_7C_{15}$ mixtures upon changing the cylinder diameter. When the diameter was 32 ($D/L_0 = 3.6$), a concentric cylindrical barrel structure (A-B-C-B-A arrangement sequence) was formed by the $A_{15}B_7/B_7C_{15}$ mixtures (Figure 13a). When the diameter was decreased to 24 ($D/L_0 = 2.7$), however, we found that the $A_{15}B_7/B_7C_{15}$ mixture was likely to form a novel screw/cylinder structure (Figure 13b). We observed that block C formed an inside core winding with helical stripes, which is similar to the screw structure. Xiang et al.[11] reported that a helical morphology was formed by polystyrene-*b*-polybutadiene copolymers in nanopores. They found that the polybutadiene blocks formed a helical structure and maintained contact with the pore walls. Recently, Wu et al.[27] studied the self-assembly of a silica−surfactant composite confined within cylindrical nanochannels; they observed a helical structure. The screw structure in our case, however, is different from those helical structures observed previously: our screw structure is composed of a cylindrical core and a screw thread. When we further decreased the cylinder diameter to 16 ($D/L_0 = 1.8$), the $A_{15}B_7/B_7C_{15}$ mixtures also formed an ordered stacked disk/cylinder structure (Figure 13d) that was similar to that of the $A_{15}B_{15}/A_{15}C_{15}$ mixtures (Figure 10d). This result means that the $A_{15}B_{15}/A_{15}C_{15}$ and $A_{15}B_7/B_7C_{15}$ mixtures can both form the same structure under suitable conditions. We calculate that the
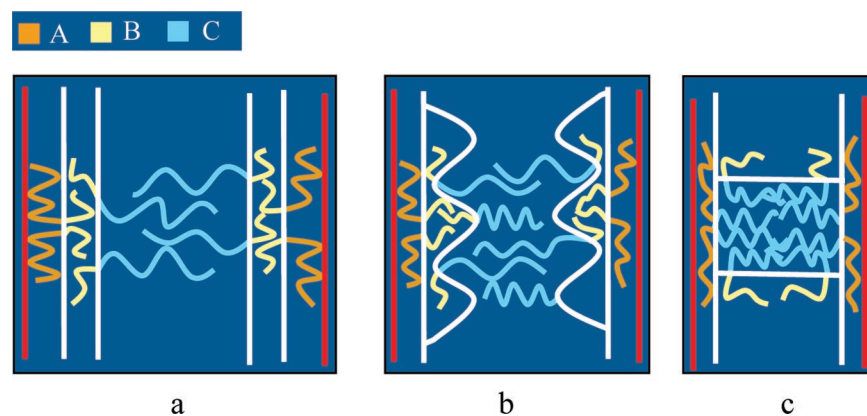
Figure 15. Schematic diagrams of the microstructures of $A_{15}B_7/B_7C_{15}$ copolymers in the cylinder with various diameters. The red and white lines refer to the cylinder wall and phase interface. (a) $D = 32$; (b) $D = 24$; (c) $D = 16$.
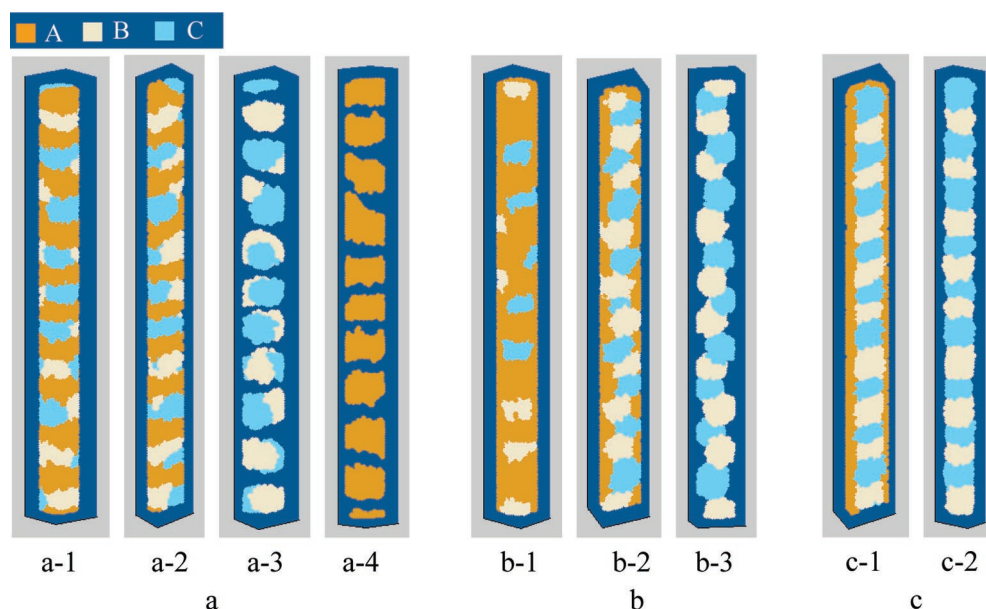
Figure 16. Morphological patterns formed from $A_{15}B_{15}/A_{15}C_{15}$ mixtures exhibiting various strengths of interactions between the boundary surfaces and the various blocks. The cylinder diameter and height were 16 and 180, respectively. (a) $\overline{\epsilon_{AD}} = -0.05$, $\overline{\epsilon_{BD}} = \overline{\epsilon_{CD}} = 0.05$, (a-1) three-dimensional structure, (a-2) section structure, (a-3) only blocks B and C, (a-4) only block A; (b) $\overline{\epsilon_{AD}} = -0.1$, $\overline{\epsilon_{BD}} = \overline{\epsilon_{CD}} = 0.1$, (b-1) three-dimensional structure, (b-2) section structure, (b-3) only blocks B and C; (c) $\overline{\epsilon_{AD}} = -0.2$, $\overline{\epsilon_{BD}} = \overline{\epsilon_{CD}} = 0.2$, (c-1) section structure, (c-2) only blocks B and C. The blue area is the background.

average thicknesses of the B and C disks were each ca. 7.5. Figure 13c indicates that when the diameter was 20 ($D/L_0 = 2.2$), the screw/cylinder and stacked disk/cylinder structures coexisted. The upper part of the cylinder exhibited a screw/cylinder structure, while the lower part adopted a stacked disk/cylinder structure. It was probable the content of block C in the upper part was somewhat higher than that in the lower part, so the C domains in the upper part of cylinder were connected together and formed the screw structure. We provide a table in the Supporting Information (Table S1) showing the structures of the $A_{15}B_{15}/A_{15}C_{15}$ and $A_{15}B_7/B_7C_{15}$ mixtures as a function of the cylinder diameter. We can clearly observe the effect of the confinement size on the self-assembled structures.

For the $A_{15}B_7/B_7C_{15}$ mixtures, upon decreasing the cylinder diameter from 32 to 16, the domain formed by block C transitioned from a cylindrical core structure to a screw structure and then to a disklike structure (Figure 13). It is obviously that the phase domain formed by block C decreases directly with decreasing the cylinder diameter. This result indicates that the degree of stretching of block C is higher in the larger cylinder. In addition, we calculated the thickness of the cylindrical A barrel for various cylinder diameters. When the cylinder

diameter was 32, the thickness of the cylindrical A barrel was about 2.3. When the cylinder diameter was decreased to 16, however, the block A formed an extremely thin barrel about 0.6. Within such an extremely thin barrel domain, the folding of block A became quite difficult. As a result, the degree of stretching of block A would increase when the cylinder diameter decreased from 32 to 16. The variations of the end-to-end distances of blocks A, B, and C with the cylinder diameter are displayed in Figure 14. It can be found that the end-to-end distance of block A increases with decreasing the diameter, whereas the end-to-end distance of block C decreases with decreasing the diameter. Moreover, it is seen that the end-to-end distance of block B is always less than those of blocks A and C. This is because the length of block B is much shorter than the lengths of blocks A and C ($L_B = 7$, $L_A = L_C = 15$). To provide greater clarity, we provide a series of schematic diagrams showing the microstructures of $A_{15}B_7/B_7C_{15}$ mixtures within the various cylinders (Figure 15).

The interactions between the boundary surfaces and the blocks are another key parameter that determines the morphologies of copolymer melts under confinement. Very recently, Chen et al.[28] investigated the effect of the surface field on the self-assembly
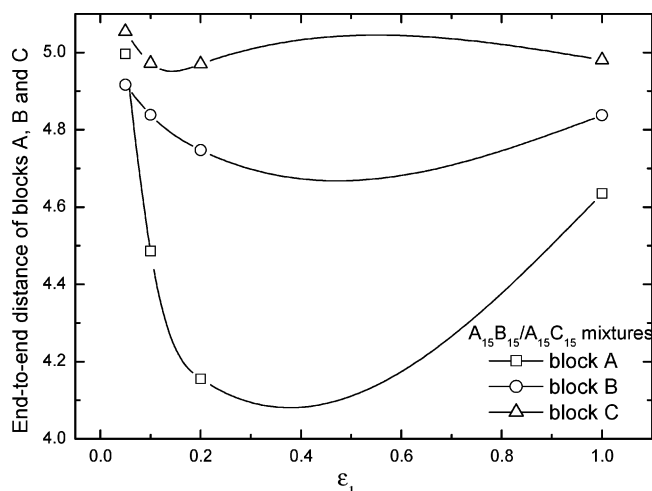
Figure 17. Variations of the end-to-end distances of blocks A, B, and C for the $A_{15}B_{15}/A_{15}C_{15}$ mixtures with the interactions between the boundary surfaces and the blocks (ϵ_1).
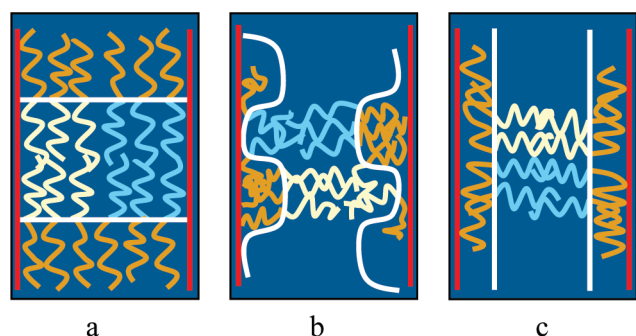

Figure 18. Schematic diagrams of the microstructures of $A_{15}B_{15}/A_{15}C_{15}$ copolymers with varying the interactions between the boundary surfaces and the blocks. The red and white lines refer to the cylinder wall and phase interface. (a) $\overline{\epsilon_{AD}} = -0.05$, $\overline{\epsilon_{BD}} = \overline{\epsilon_{CD}} = 0.05$; (b) $\overline{\epsilon_{AD}} = -0.1$, $\overline{\epsilon_{BD}} = \overline{\epsilon_{CD}} = 0.1$; (c) $\overline{\epsilon_{AD}} = -0.2$, $\overline{\epsilon_{BD}} = \overline{\epsilon_{CD}} = 0.2$.

of a symmetric diblock copolymer under cylindrical confinement; they observed a variety of morphologies including stacked disk, single-helix, catenoid-cylinder, gyroidal, stacked circle,

and concentric cylindrical barrel structures. In our present study, we also examined the effects of the interactions between the boundary surfaces and the blocks on the self-assembled morphologies. In Figure 16, we present a series of self-assembled morphologies of $A_{15}B_{15}/A_{15}C_{15}$ mixtures within cylinders ($D = 16$) that were obtained after varying the interactions between the boundary surfaces and the blocks. When $\epsilon_1 = 0.05$ ($\overline{\epsilon_{AD}} = -0.05$, $\overline{\epsilon_{BD}} = \overline{\epsilon_{CD}} = 0.05$), we observed that the $A_{15}B_{15}/A_{15}C_{15}$ mixtures formed a stacked disk structure (Figure 16a) with an alternating arrangement sequence of A and BC disks. In addition, it is quite interesting to note that the BC disks comprised B and C microdomains. The calculated average thicknesses of both the A and BC disks were ca. 9. Upon further increasing the value of ϵ_1 to 0.1 ($\overline{\epsilon_{AD}} = -0.1$, $\overline{\epsilon_{BD}} = \overline{\epsilon_{CD}} = 0.1$), however, blocks B and C formed a novel stacked-sphere core in the center of the cylinder and maintained contact with the boundary surfaces, as indicated in Figure 16b. In addition, it is interesting to note that the core was formed by stacked A and B spheres in an alternating arrangement sequence. Upon further increasing the interactions energy between the boundary surfaces and the blocks ($\epsilon_1 = 0.2$, $\overline{\epsilon_{AD}} = -0.2$, $\overline{\epsilon_{BD}} = \overline{\epsilon_{CD}} = 0.2$), Figure 16c indicates that the $A_{15}B_{15}/A_{15}C_{15}$ mixtures formed the same stacked disk/cylinder structure (Figure 10d).

Upon increasing the value of ϵ_1 from 0.05 to 0.2, the domain formed by block A transitioned from a disklike structure to a faulty cylindrical barrel structure embedded with some B and C domains and then to a complete cylindrical barrel structure (Figure 16). The variations of the end-to-end distances of blocks A, B, and C with the value of ϵ_1 are presented in Figure 17. It is seen that the end-to-end distance of block A decreases with increasing the value of ϵ_1 at first and then increases with further increasing the value of ϵ_1. Figure 18 provides a series of schematic diagrams showing the microstructures of $A_{15}B_{15}/A_{15}C_{15}$ mixtures with varying the interaction energies (ϵ_1) between the boundary surfaces and the blocks. The diagrams show us why the block A is more coiled in the case of $\epsilon_1 = 0.1$ (Figure 16b).

Figure 19 displays a series of typical morphologies formed by the $A_{15}B_7/B_7C_{15}$ mixtures in a cylinder ($D = 16$) upon
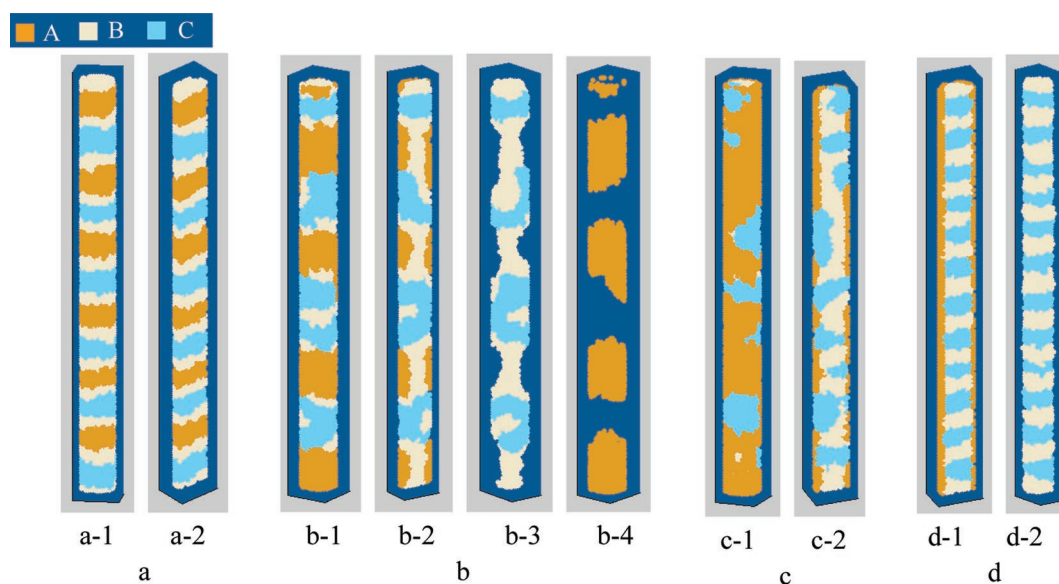
Figure 19. Morphological patterns formed from $A_{15}B_7/B_7C_{15}$ mixtures exhibiting various strengths of interactions between the boundary surfaces and the blocks. The cylinder diameter and height were 16 and 180, respectively. (a) $\overline{\epsilon_{AD}} = \overline{\epsilon_{BD}} = \overline{\epsilon_{CD}} = 0$, (a-1) three-dimensional structure, (a-2) section structure; (b) $\overline{\epsilon_{AD}} = -0.1$, $\overline{\epsilon_{BD}} = \overline{\epsilon_{CD}} = 0.1$, (b-1) three-dimensional structure, (b-2) section structure, (b-3) only blocks B and C, (b-4) only blocks A; (c) $\overline{\epsilon_{AD}} = -0.2$, $\overline{\epsilon_{BD}} = \overline{\epsilon_{CD}} = 0.2$, (c-1) three-dimensional structure, (c-2) section structure; (d) $\overline{\epsilon_{AD}} = -0.4$, $\overline{\epsilon_{BD}} = \overline{\epsilon_{CD}} = 0.4$, (d-1) section structure, (d-2) only blocks B and C. The blue area is the background.
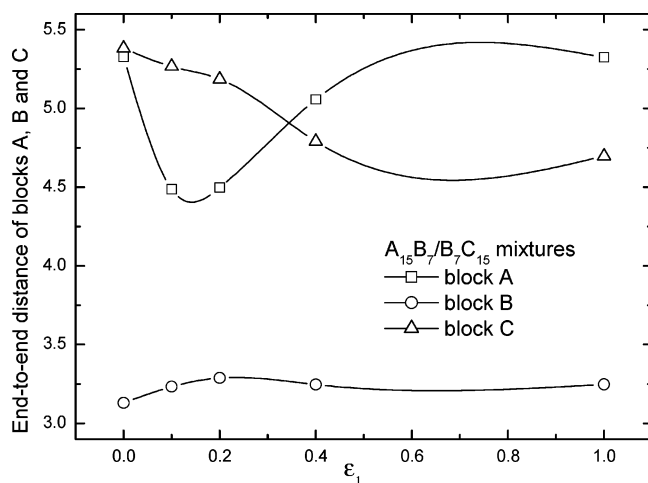
Figure 20. Variations of the end-to-end distances of blocks A, B, and C for the $A_{15}B_7/B_7C_{15}$ mixtures with the interactions between the boundary surfaces and the blocks (ϵ_1).

Figure 21. Schematic diagrams of the microstructures of $A_{15}B_7/B_7C_{15}$ copolymers with varying the interactions between the boundary surfaces and the blocks. The red and white lines refer to the cylinder wall and phase interface. (a) $\overline{\epsilon_{AD}} = 0$, $\overline{\epsilon_{BD}} = \overline{\epsilon_{CD}} = 0$; (b) $\overline{\epsilon_{AD}} = -0.1$, $\overline{\epsilon_{BD}} = \overline{\epsilon_{CD}} = 0.1$; (c) $\overline{\epsilon_{AD}} = -0.4$, $\overline{\epsilon_{BD}} = \overline{\epsilon_{CD}} = 0.4$.

varying the interaction energies between the boundary surfaces and the blocks. At $\epsilon_1 = 0$ ($\overline{\epsilon_{AD}} = \overline{\epsilon_{BD}} = \overline{\epsilon_{CD}} = 0$), we found that the $A_{15}B_7/B_7C_{15}$ mixtures were arranged to form a stacked disk structure (Figure 19a) with a different alternating arrangement sequence (A-B-C sequence). The average thickness of the B disk was ca. 4.8, whereas the average thicknesses of the A and C disks were ca. 10.2. When a slightly stronger interaction existed between the boundary surfaces and the blocks ($\epsilon_1 = 0.1$, $\overline{\epsilon_{AD}} = -0.1$, $\overline{\epsilon_{BD}} = \overline{\epsilon_{CD}} = 0.1$), we observed a novel catenoid-cylinder structure (Figure 19b). In addition, from Figure 19b-3, we observe that block B formed a bottleneck structure to connect the separated cylindrical BC domains. In this study, the surfaces of the cylinder wall repulsed blocks B and C but attracted block A. When the interactions between the surfaces and the blocks were weak ($\overline{\epsilon_{AD}} = -0.1$, $\overline{\epsilon_{BD}} = \overline{\epsilon_{CD}} = 0.1$), the interactions among blocks A, B, and C ($\overline{\epsilon_{AB}} = \overline{\epsilon_{AC}} = \overline{\epsilon_{BC}} = 0.5$) were the dominant factor that determined the morphology. As a result, in the area with high contents of blocks B and C, blocks B and C formed some separated cylindrical BC domains and maintained contact with the cylinder walls. However, in the area with high content of block A, block A formed the cylindrical barrels, and block B formed the inside bottleneck-like core. When a stronger interaction exists, however, between the boundary surfaces and the blocks ($\epsilon_1 = 0.2$, $\overline{\epsilon_{AD}} = -0.2$, $\overline{\epsilon_{BD}} = \overline{\epsilon_{CD}} = 0.2$), we found (Figure 19c) that the $A_{15}B_7/B_7C_{15}$ mixtures formed a coexisting catenoid-cylinder and stacked disk/cylinder structure. At $\epsilon_1 = 0.4$ ($\overline{\epsilon_{AD}} = -0.4$, $\overline{\epsilon_{BD}} = \overline{\epsilon_{CD}} = 0.4$), the stacked disk/cylinder structure reappeared (Figure 19d).

Upon increasing the value of ϵ_1 from 0 to 0.4, the domain formed by block A transitioned from a disklike structure to some short cylindrical barrel structures and then to an extremely thin cylindrical barrel structure, as shown in Figure 19a−d. Figure 20 gives the variations of end-to-end distances of blocks A, B, and C with the value of ϵ_1. It is seen that the end-to-end distance of block A decreases with increasing the value of ϵ_1 at first and then increases with further increasing the value of ϵ_1. Moreover, the end-to-end distance of block C decreases considerably with increasing the value of ϵ_1. Figure 21 shows the schematic diagrams showing the transition of microstructures of $A_{15}B_7/B_7C_{15}$ mixtures within the cylinder with varying the interaction energies.

We provide a summary of the self-assembled structures formed from the $A_{15}B_{15}/A_{15}C_{15}$ and $A_{15}B_7/B_7C_{15}$ mixtures within a cylinder ($D = 16$) as a function of the interaction energy (ϵ_1)
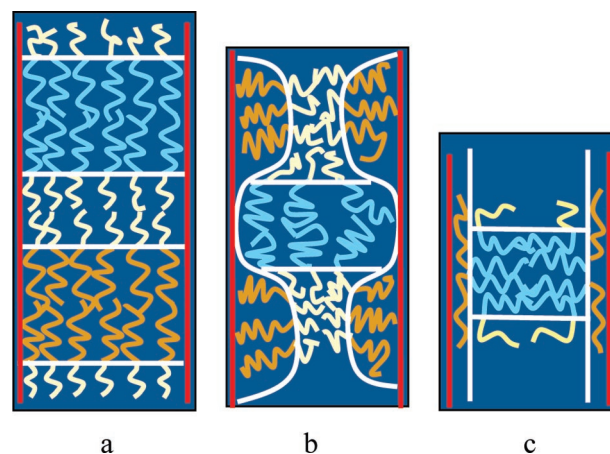
between the boundary surface and the blocks in Supporting Information (Table S2). To the best of our knowledge, the following morphologies have not yet to be observed from the self-assembly of copolymers under confinement: double helix/cylinder (Figure 10a), stacked disk/cylinder (Figure 10d), screw/cylinder (Figure 13b), stacked disks of alternating A and BC disks (Figure 16a), stacked disks of alternating A, B, and C disks (Figure 19a), BC stacked sphere/cylinder (Figure 16b), and catenoid-cylinder (Figure 19b) structures. We hope that our results will provide motivation for related experimental studies that may aid in the further understanding of the phase structures of block copolymers confined on the nanoscale.

4. Conclusion

We have employed a Monte Carlo method to study the self-assembly of diblock copolymer mixtures within cylindrically confined states. We found that mixtures of the copolymers form more complex self-assembled structures than do their individual components. By adjusting the cylinder diameter and the interaction energy between the boundary surfaces and the blocks, we discovered a rich variety of self-assembled structures. Upon decreasing the cylinder diameter, the self-assemble structures formed by $A_{15}B_{15}/A_{15}C_{15}$ mixtures transitioned from double-helix/cylinder structures to stacked disk/cylinder structures, whereas the self-assembled structures of the $A_{15}B_7/B_7C_{15}$ mixtures transitioned from concentric cylindrical barrel structures to screw/cylinder structures and then to stacked disk/cylinder structures. Moreover, upon increasing the interaction energy between the boundary surfaces and the blocks, the self-assembled structures formed by $A_{15}B_{15}/A_{15}C_{15}$ mixtures transitioned from stacked disk structures to BC stacked sphere/cylinder structures and then to stacked disk/cylinder structures, whereas the self-assembled structures of $A_{15}B_7/B_7C_{15}$ mixtures transitioned from stacked disk structures to catenoid-cylinder structures and then to stacked disk/cylinder structures. In addition, we have investigated the microstructures of the self-assembled structures and found that the chain conformation and packing model were deferent for different structures.

Supporting Information Available: The summaries (Tables S1−S2) of the structures of the $A_{15}B_{15}/A_{15}C_{15}$ and $A_{15}B_7/B_7C_{15}$ mixtures as a function of the cylinder diameter and the interaction energy (ϵ_1) between the boundary surface and the blocks, the interpretation for why the total layers thicknesses obtained by the statistic method is smaller than the pore diameter. This material is available free of charge via the Internet at http://pubs.acs.org.

References and Notes

(1) Böltau, M.; Walheim, S.; Mlynek, J.; Krausch, G.; Steiner, U. *Nature* **1998**, *391*, 877−879.

(2) Kellogg, G. J.; Walton, D. G.; Mayes, A. M.; Lambooy, P.; Russell, T. P.; Gallagher, P. D.; Satija, S. K. *Phys. Rev. Lett.* **1996**, *76*, 2503−2506.

(3) Morkved, T. L.; Lu, M.; Urbas, A. M.; Ehrichs, E. E.; Jaeger, H. M.; Mansky, P.; Russell, T. P. *Science* **1996**, *273*, 931−933.

(4) Wang, Q.; Yan, Q.; Nealey, P. F.; de Pablo, J. J. *Macromolecules* **2000**, *33*, 4512−4525.

(5) Wang, Q.; Yan, Q.; Nealey, P. F.; de Pablo, J. J. *J. Chem. Phys.* **2000**, *112*, 450−464.

(6) Geisinger, T.; Müller, M.; Binder, K. *J. Chem. Phys.* **1999**, *111*, 5241−5250.

(7) Geisinger, T.; Müller, M.; Binder, K. *J. Chem. Phys.* **1999**, *111*, 5251−5258.

(8) Rockford, L.; Liu, Y.; Mansky, P.; Russell, T. P.; Yoon, M.; Mochrie, S. G. J. *Phys. Rev. Lett.* **1999**, *82*, 2602−2605.

(9) Shin, K.; Xiang, H.; Moon, S. I.; Kim, T.; McCarthy, T. J.; Russell, T. P. *Science* **2004**, *306*, 76−76.

(10) Xiang, H.; Shin, K.; Kim, T.; Moon, S. I.; McCarthy, T. J.; Russell, T. P. *Macromolecules* **2004**, *37*, 5660−5664.

(11) Xiang, H.; Shin, K.; Kim, T.; Moon, S. I.; McCarthy, T. J.; Russell, T. P. *J. Polym. Sci., Part B: Polym. Phys.* **2005**, *43*, 3377−3383.

(12) Xiang, H.; Shin, K.; Kim, T.; Moon, S. I.; McCarthy, T. J.; Russell, T. P. *Macromolecules* **2005**, *38*, 1055−1056.

(13) Sun, Y.; Steinhart, M.; Zschech, D.; Adhikari, R.; Michler, G. H.; Gösele, U. *Macromol. Rapid Commun.* **2005**, *26*, 369−375.

(14) He, X.; Song, M.; Liang, H.; Pan, C. *J. Chem. Phys.* **2001**, *114*, 10510−10513.

(15) Sevink, G. J. A.; Zvelindovsky, A. V.; Fraaije, J. G. E. M.; Huinink, H. P. *J. Chem. Phys.* **2001**, *115*, 8226−8230.

(16) Li, W.; Wickham, R. A.; Garbary, R. A. *Macromolecules* **2006**, *39*, 806−811.

(17) Yu, B.; Sun, P.; Chen, T.; Jin, Q.; Ding, D.; Li, B.; Shi, A. *Phys. Rev. Lett.* **2006**, *96*, 138306.

(18) Feng, J.; Ruckenstein, E. *Macromolecular,* **2006**, *39*, 4899−4906.

(19) Binder, K.; Hermann, D.K. *Monte Carlo Simulation in Statistical Physics.* Springer: Heidelberg, 1988.

(20) Larson, R. G.; Scriven, L. E.; Davis, H. T. *J. Chem. Phys.* **1985**, *83*, 2411−2420.

(21) Larson, R. G. *J. Chem. Phys.* **1989**, *91*, 2479−2488.

(22) Carmesin, I.; Kremer, K. *Macromolecules* **1988**, *21*, 2819−2823.

(23) Metropolis, N.; Rosenbluth, A. W.; Rosenbluth, M. N.; Teller, A. H.; Teller, E. *J. Chem. Phys.* **1953**, *21*, 1087−1092.

(24) Sariban, A.; Binder, K. *Macromolecules* **1988**, *21*, 711−726.

(25) Elbs, H.; Abetz, V.; Hadziioannou, G.; Drummer, C.; Krausch, G. *Macromolecules* **2001**, *34*, 7917−7919.

(26) Elbs, H.; Drummer, C.; Abetz, V.; Krausch, G. *Macromolecules* **2002**, *35*, 5570−5577.

(27) Wu, Y.; Cheng, G.; Katsov, K.; Sides, S. W.; Wang, J.; Tang, J.; Fredrickson, G. H.; Moskovits, M.; Stucky, G. D. *Nat. Mater.* **2004**, *3*, 816−822.

(28) Chen, P.; He, X.; Liang, H. *J. Chem. Phys.* **2006**, *124*, 104906−1−6.